metals

MDPI

Article

Effect of Nd on Functional Properties of Biodegradable Zn Implants in In Vitro Environment

Efrat Hazan-Paikin, Lital Ben Tzion-Mottye, Maxim Bassis, Tomer Ron * and Eli Aghion

Department of Materials Engineering, Ben-Gurion University of the Negev, Beer-Sheva 8410501, Israel; hazanefr@post.bgu.ac.il (E.H.-P.); bentzlit@post.bgu.ac.il (L.B.T.-M.); maximba@post.bgu.ac.il (M.B.); egyon@bgu.ac.il (E.A.)

* Correspondence: toron@post.bgu.ac.il

Abstract: The present study aims to evaluate the effect of up to 3 wt.% Nd on pure Zn in terms of physical properties and in vitro analysis. The use of Nd as an alloying element is due to its relatively adequate biocompatibility and its potential capability to reinforce metals with a hexagonal close-packed (HCP) crystal structure, such as Mg and Zn. The microstructural assessment was executed using X-ray diffraction analysis, along with optical and scanning electron microscopy. The mechanical properties were evaluated by hardness and tensile strength testing. The corrosion performance in simulated physiological environments was examined by means of immersion tests, potentiodynamic polarization, and impedance spectroscopy using phosphate-buffered saline (PBS) solution. Cytotoxicity assessment was carried out by indirect cell viability analysis according to the ISO 10993-5/12 standard using Mus musculus 4T1 cells, which are known to be very sensitive to toxic environments. The obtained results clearly highlighted the reinforcing effect of Nd in Zn-base alloys, mainly due to the formation of a secondary phase: $NdZn_5$. This strengthening effect was acquired without impairing the inherent ductility and corrosion performance of the tested alloys. The cytotoxicity assessment indicated that the addition of Nd has a strong favorable effect on cell viability, which stimulates the inherent anti-inflammatory characteristics of Zn.

Keywords: biodegradable implants; in vitro; cell viability; zinc; Zn-Nd

check for updates

Citation: Hazan-Paikin, E.; Ben Tzion-Mottye, L.; Bassis, M.; Ron, T.; Aghion, E. Effect of Nd on Functional Properties of Biodegradable Zn Implants in In Vitro Environment. *Metals* **2024**, *14*, 655. https://doi.org/10.3390/met14060655

Received: 30 April 2024
Revised: 29 May 2024
Accepted: 30 May 2024
Published: 31 May 2024

Copyright: © 2024 by the authors. Licensee MDPI, Basel, Switzerland. This article is an open access article distributed under the terms and conditions of the Creative Commons Attribution (CC BY) license (https://creativecommons.org/licenses/by/4.0/).

1. Introduction

Implants with adequate biocompatibility and mechanical properties, and with acceptable overall performance in physiological environments, are required to bind bones and tissues and to assist in healing processes using various medical devices [1,2]. Numerous metals and alloys are used as structural materials for these implants and are divided into two main categories: permanent implants and biodegradable implants. Permanent implants, such as those made from stainless steels and Ti-base alloys, exhibit extremely high strength, excellent corrosion resistance, and nearly endless durability. The disadvantages of permanent implants relate to their possible detrimental effect on the immune system, premature mechanical failure due to stress corrosion, and stress shielding in orthopedic applications that required secondary surgery. In contrast, biodegradable implants can degrade and be absorbed post implantation while maintaining their mechanical integrity during the critical period before complete healing is achieved [3–6]. In many cases, the use of a temporary biodegradable implant is sufficient as there is no need for the presence of the implant after the recovery of the tissue [6–11]. The desired time for the biodegradable implant to remain in the body until complete dissolution varies, depending on the function of the implant and the tissue to which it is attached. This time can be controlled, mainly by modifying the chemical composition and processing methods of the biodegradable metal implant, which regulate the corrosion performance in physiological environments.

The most studied biodegradable metals in the last couple of decades were Fe and Mg, mainly due to their inherent biocompatibility. However, critical limitations were

revealed in terms of their suitability for medical applications. Fe displays a relatively slow corrosion rate for a practical biodegradable implant. Further, part of its corrosion products may be toxic, and their voluminous mass tends to reject neighboring tissues, which might encourage inflammatory processes [11–19]. Mg suffers from an accelerated corrosion rate and reduces mechanical strength, which are not compatible with regular implant requirements. In addition, during the disintegration, Mg produces hydrogen gas that can penetrate the blood circulation and provoke dangerous gas embolism [18–35]. Recently, Zn and Zn-based alloys have been considered as promising alternatives to Mg and Fe. This is mainly attributed to the inherent excellent biocompatibility of Zn, and its essential role in many physiological reactions in the human body such as participating in critical nucleic acid metabolism and gene countenance [36]. Nevertheless, it should be indicated that although low levels of Zn are not considered a toxic substance, high levels can provoke toxicity and cause anemia [25]. Furthermore, Zn has a significant beneficial effect in terms of antibacterial capabilities that can prevent acute infection post implantation. However, the main disadvantage of Zn relates to its reduced strength and limitations in terms of degradability that may not be sufficient for practical medical applications [37–44]. Hence, the present study aims to evaluate the potential of innovative Zn-based alloys with up to 3%Nd as structural materials for biodegradable implants. The selection of a minor amount of Nd as an alloying element is related to its relatively adequate biocompatibility and its ability to reinforce metals such as Mg and Zn that have an HCP structure [45–47]. Nevertheless, it should be pointed out that the bioaccumulation of Nd in humans (at high Nd levels) can provoke liver, kidney, and heart toxicity [48,49].

2. Experimental Methods

2.1. Preparation of Tested Alloys

Zn-based alloys with different amounts of Nd (up to about 3 wt.%) were produced by gravity casting within a graphite crucible using high-purity Zn bars and Nd powder with an average grain size of 50 μm. The casting process was performed at 700 °C for two hours, along with active stirring every half hour to obtain a uniform and fully synthesized alloy. A rectangular steel die that was pre-heated to 400 °C was employed for the solidification process of the alloys. Post solidification, the cast alloys were quenched in cold water. The mean chemical composition of the prepared alloys derived from X-ray fluorescence wavelength-dispersive (WDXRF) spectrometry is shown in Table 1 (Axios (1 kW) with SuperQ version 5 software, PANalytical B.V. Almelo, The Netherlands). Prior to the final extrusion process, the alloy was homogenized at 200 °C for two hours. Following this heat treatment, the rods were extruded at 350 °C from a 16 mm to a 6 mm diameter, which comprises an extrusion ratio of about $2\frac{2}{3}$. The extrusion process aims to upgrade the mechanical properties of the tested alloys by eliminating inherent casting defects (mainly in the form of porosity) [50,51].

Table 1. The average chemical composition of the prepared alloys (wt.%).

Tested Alloy	Nd	S	Zn
Zn-1%Nd	0.9	0.082	Bal.
Zn-2%Nd	2.4	0.102	Bal.
Zn-3%Nd	3.1	0.067	Bal.

2.2. Microstructure Analysis

The microstructure examination was carried out using three research tools: (i) optical microscopy (ICP-SPECTRO, ARCOS FHS-12, Kelve, Germany) for general observation; (ii) scanning electron microscopy (SEM) (JEOL-5600, JEOL Ltd., Tokyo, Japan) equipped with an energy-dispersive X-ray spectroscopy (EDS) detector (Thermo Fisher Scientific, Waltham, MA, USA) for in-depth analysis of the different phases, as well as for spot chemical examination [52]; and (iii) X-ray diffraction (XRD) analysis (2100 RIGAKU, Tokyo,

Japan), employing a Cu-Kα diffractometer (40 kV, 30 mA) at a scanning rate of 0.02°/min, for phase identification. Prior to the microscopical analysis, the test samples were polished and etched using a NaOH-based solution (10 g NaOH and 100 mL water) [53].

2.3. Mechanical Properties

Hardness and tensile strength examinations were conducted to assess the mechanical properties of the investigated alloys. Hardness testing was carried out using Vickers analysis (Zwick/Roell Indentec, ZwickRoell Ltd., Worcester, UK) under a load of 5 kg (HV5). Tensile strength testing was executed using a CORMET system (C76, Testing Systems, Vantaa, Finland), while maintaining a constant strain of 0.5 mm per minute.

2.4. Corrosion Resistance and Electrochemical Performance

The corrosion resistance of the tested alloys in equilibrium conditions was evaluated by a conventional immersion test. The samples for this test in the form of elongated cylinders with a 10 mm diameter and 8 mm length were cut using an electro-erosion cutting machine (EDM, ARTA 123 pro, NPK "Delta-Test", Fryazino, Russia). The simulated physiological environment was in the form of a phosphate-buffered saline (PBS) solution (1 tablet per 200 mL of water), while the test temperature was 37 °C and the test duration was 14 days, which aligns with the ASTM G31-72 standard [54]. The pH level of the PBS solution was maintained at around 7.4, which is quite like the ideal pH of the human body [55]. The corrosion rate in terms of mm/year was evaluated by removing and measuring the corrosion products using an ultrasonic bath and ethanol, and employing the following equation:

$$CR = \frac{W}{A \cdot t \cdot \rho} \quad (1)$$

where CR is the corrosion rate, W is the weight loss, A is the area exposed to corrosion, t is the duration time, and ρ is the density of the sample.

The electrochemical performance of the alloys was investigated using potentiodynamic polarization and impedance spectroscopy analysis (EIS). These examinations were carried out by a Bio Logic SP-200 potentiostat (BioLogic Science Instruments, Seyssinet-Pariset, France) equipped with EC-Lab software V11.18. Prior to the electrochemical analysis, the post-extruded samples were thoroughly cleaned and polished to 1200 grit. The three-electrode-cell facility that was used for the examinations included a saturated calomel reference electrode (SCE), a platinum counter-electrode, and a working electrode in the form of the tested sample [54]. The exposed area of the working electrode was 1 cm^2 and the corrosive environment was in the form of a PBS solution at room temperature. The scanning rate of the potentiodynamic polarization measurements was 1 mV/s, and EIS measurements were carried out between 10 kHz and 100 MHz at a 10 mV amplitude over the open-circuit potential. The corrosion rate was calculated by Tafel extrapolation [54].

2.5. Cytotoxicity Evaluation

The cytotoxicity evaluation of the alloys was carried out by evaluating the effect of indirect extract cell metabolic activity according to the ISO 10993-5/12 standard [56]. Mus musculus 4T1 cells were selected for the cytotoxicity extermination owing to their inherently increased sensitivity to toxic effects compared to primary cells [20]. The samples for the test were cut by an electro-erosion cutting machine (EDM, ARTA 123 pro), in the form of cylinders with a 10 mm diameter and 2 mm length. The tested samples included 4 samples from each of the tested alloys, along with 4 samples of Ti-6Al-4V that is considered to have excellent biocompatibility and hence can be used as a reference metal. The preparation of the samples included polishing up to 4000 grit, cleaning in ethanol for 10 min, washing in acetone for 5 min, drying in air, and sterilizing in UV light for 1 h on both sides of the sample. The samples were immersed for 24 h in the required extract that is called "Medium" and incubated in a 5% CO_2 humidified atmosphere at 37 °C. This Dulbecco's Modified Eagle's Medium (DMEM) included 4.5 g of L−1 D-Glucose, 4 mM L-Glutamine, 10% Fetal

Bovine Serum (FBS), 1 mM Sodium Pyruvate, and a 1% Penicillin–Streptomycin–Neomycin (PSN) antibiotic mixture. The surface-area-to-volume ratio extraction was 1.25 cm^2 per 1 mL. The cells were seeded in two 96-well tissue plates with the required extract for 24 h. The density of the seeding was 5000 cells per well, in order to allow the attachment of the cells to the surface. After 24 h, the liquids from all the cell plates were collected and replaced with 100 µL of filtered alloy extract obtained by filtration through a PVDF membrane (0.45 µm). To bridge the gap between the in vitro and in vivo conditions, the concentration of the filtered alloy extract was 10%, while the rest was the medium [57]. The cytotoxicity analysis requires 2 control groups for testing, one positive for non-toxic evaluation and one negative for toxic evaluation. The positive control group contained cell wells with only DMEM and the negative control group contained 90% DMEM and 10% DMSO. This process was carried out on two identical 96-well plates that were incubated for 24 and 48 h, respectively. After 24 and 48 h, the general appearance of each sample in the two 96-well plates was visually evaluated using a CoolLED pE-2 collimator fitted to an inverted phase-contrast microscope (Eclipse, Nikon, Tokyo, Japan) equipped with a digital camera (DS-Qi1Mc, Nikon, Tokyo, Japan). The cell metabolic activity was assessed after 24 and 48 h, by using a cell proliferation kit (XTT, Biological Industry, Beit Haemek, Israel) and a microplate reader (SYNERGY-Mx, BioTek, Winooski, VT, USA).

All the liquids from the cell plates were collected and replaced with 50 µL of reagent and 1 µL of activator versus 100 µL of DMEM for each well, with 2 h of incubation. The color of the formation liquid from the cells was measured spectrophotometrically at 490 nm, using a microplate reader. The measured values were compared with the control blank wells to evaluate the cell viability. The cell viability was calculated according to the following equation:

$$Viability\ [\%] = \frac{OD_{sample}}{OD_{control}} \cdot 100\% \quad (2)$$

where *ODsample* represents the optical density calculated from the cells cultured with the tested extracts, and *ODcontrol* is the optical density calculated from the cells in the control culture media.

3. Results

The phase identification of the tested alloys obtained by XRD analysis clearly indicates the presence of two major phases, pure Zn and a Nd-rich phase, as shown in Figure 1. The Nd-rich phase was identified as $NdZn_5$ [58]. The intensity of the Nd-rich phase rose as the Nd content was increased from 1% to 3%.

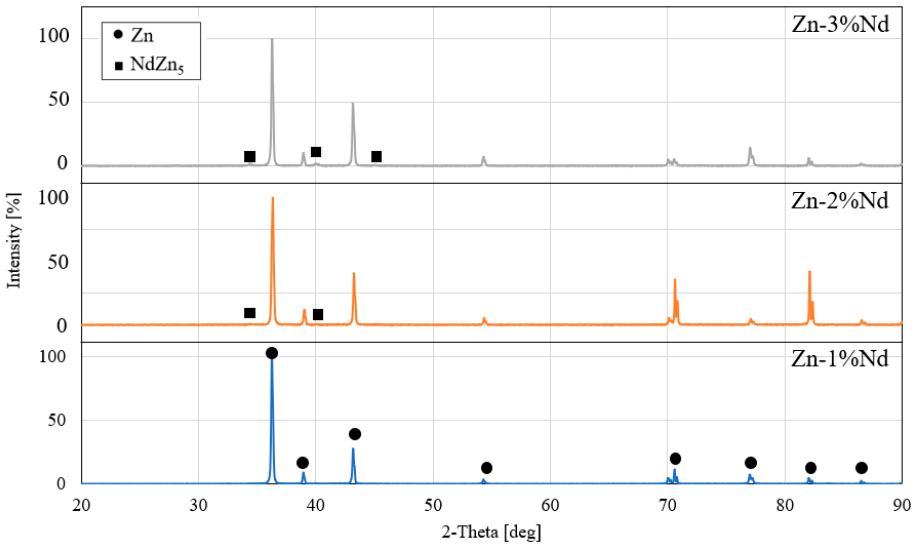


Figure 1. XRD analysis of pure Zn with up to 3%Nd (diffraction file numbers: Nd 00-004-0831, $NdZn_5$ 00-027-0325).

The microstructure of the tested alloys in as-cast conditions and post extrusion, characterized by optical and SEM microscopy, is shown in Figures 2 and 3, respectively. It is evident that the presence of enlarged porosity in the as-cast conditions, especially in alloys containing a higher amount of Nd (2–3%), was significantly reduced post extrusion—as expected. In general, the amount of the secondary Nd-rich phase ($NdZn_5$) scattered within the Zn-base matrix increased as the Nd content was raised from 1% to 3%. The reduced amount of the secondary phase in the Zn-1%Nd alloy may explain the difficulty in detecting this phase by the XRD analysis. In addition, the size of the secondary Nd-rich phase was significantly increased from less than 5 µm in the Zn-1%Nd alloy to nearly 35 µm in the Zn-3%Nd alloy. The coarsening of such a secondary phase in metals with an HCP structure, like Zn-base alloys, is relatively common [59].

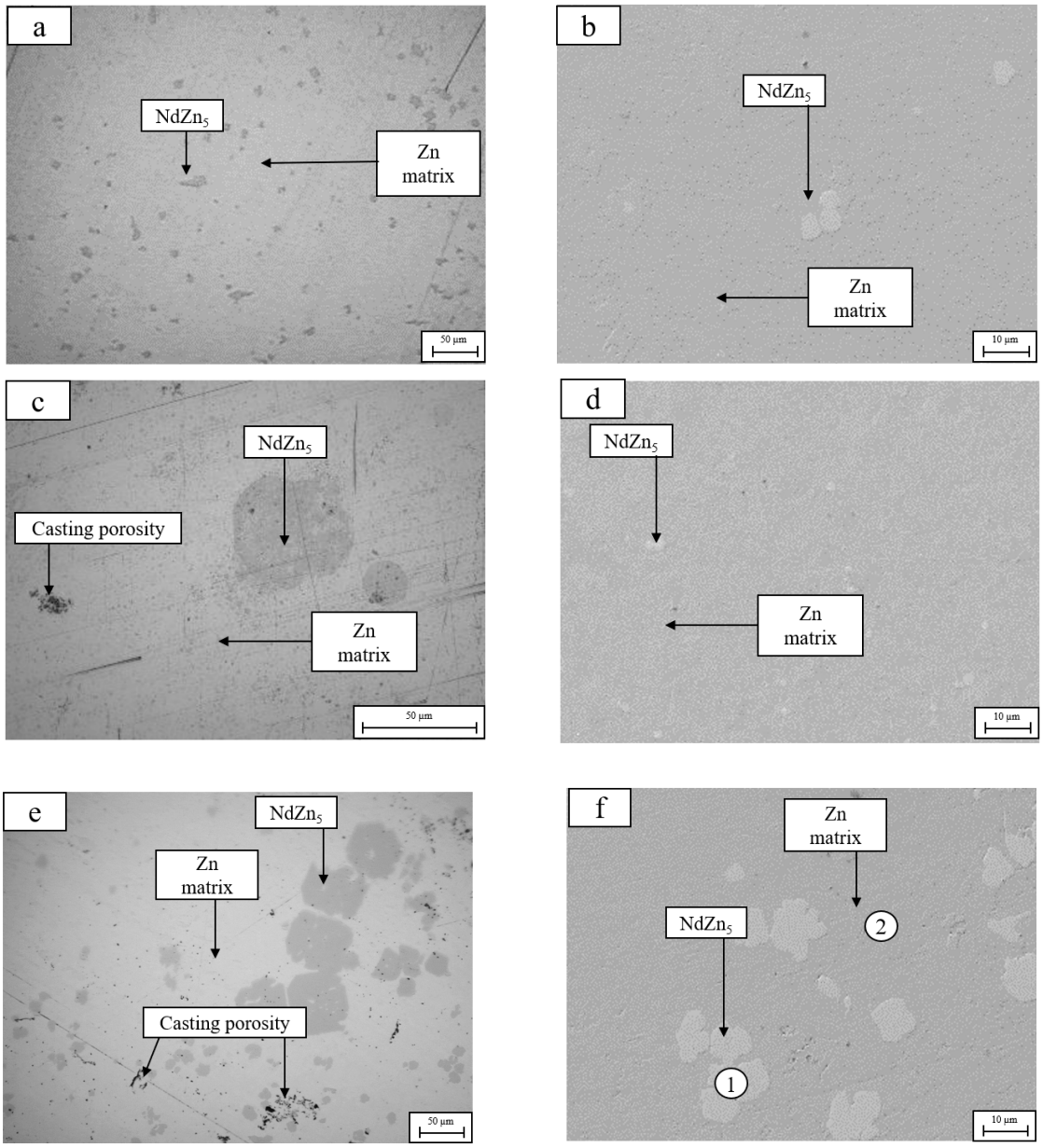


Figure 2. Typical microstructures of Zn with up to 3%Nd in as-cast conditions obtained by optical and SEM microscopy: (**a**) optical Zn-1%Nd; (**b**) SEM Zn-1%Nd; (**c**) optical Zn-2%Nd; (**d**) SEM Zn-2%Nd; (**e**) optical Zn-3%Nd; (**f**) SEM Zn-3%Nd.

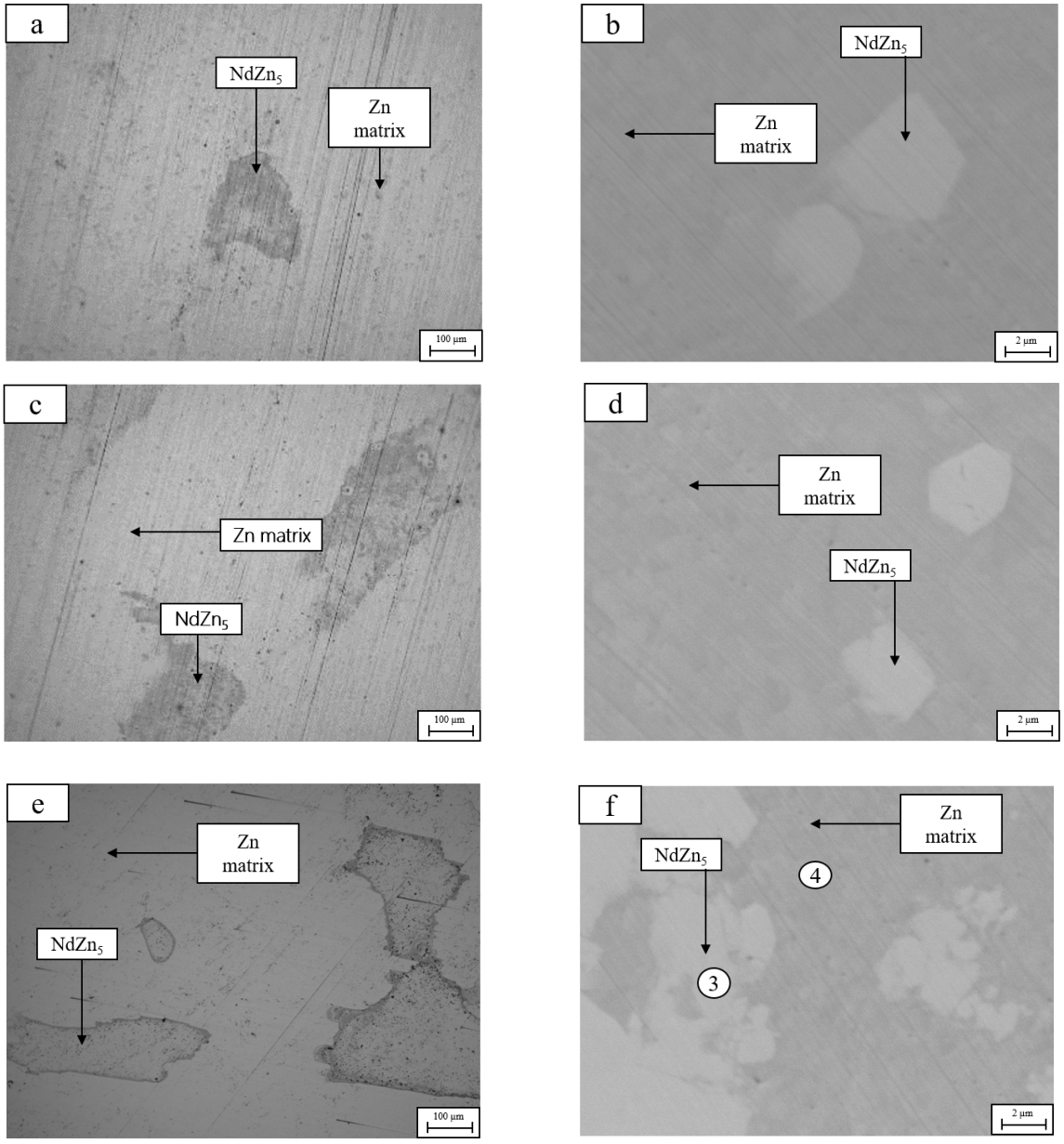


Figure 3. Typical microstructures of Zn with up to 3%Nd post extrusion obtained by optical and SEM microscopy: (**a**) optical Zn-1%Nd; (**b**) SEM Zn-1%Nd; (**c**) optical Zn-2%Nd; (**d**) SEM Zn-2%Nd; (**e**) optical Zn-3%Nd; (**f**) SEM Zn-3%Nd.

The spot chemical analysis of the secondary Nd-rich phase ($NdZn_5$) in the Zn-3%Nd alloy by SEM-EDS examination, in as-cast conditions and post extrusion, is shown in Table 2. This reveals that the secondary phase was clearly enriched in Nd with an amount of about 6%.

Table 2. Localized chemical composition by EDS analysis of Zn-3%Nd alloy related to Figures 2f and 3f.

Point of Measurement	Zn (wt.%)	Nd (wt.%)	Dominant Phases
1	94.0	6.0	$NdZn_5$
2	99.4	0.6	Zn-base matrix
3	93.2	6.8	$NdZn_5$
4	99.8	0.2	Zn-base matrix

The mechanical properties of Zn with up to 3%Nd in terms of hardness and tensile strength are shown in Figure 4 and Table 3, respectively. We can observe that the hardness of the tested alloys was increased as the Nd content was increased from 1 to 3%. The mechanical properties show that the yield point (YP) and ultimate tensile strength (UTS) were both increased, along with slight ductility elevation in terms of elongation, as the Nd content was increased.

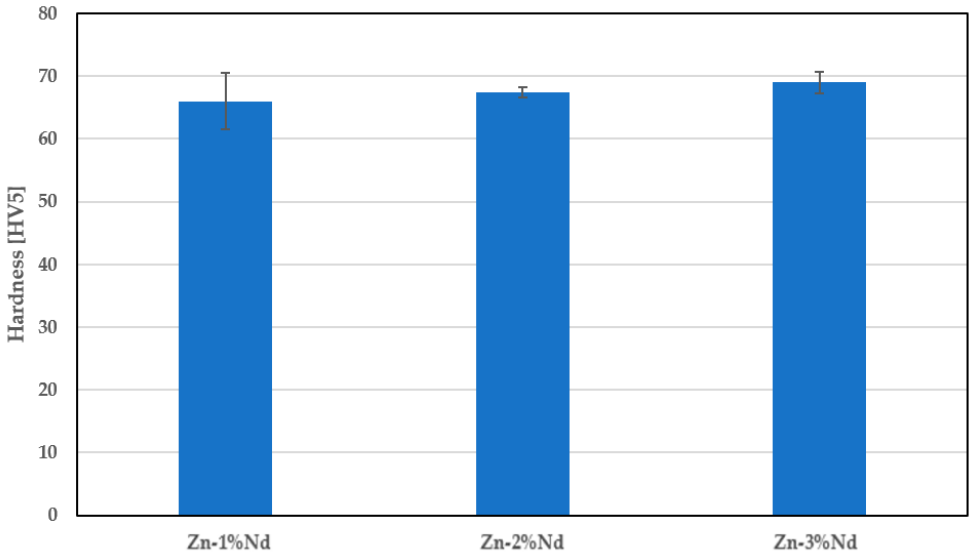


Figure 4. Hardness measurement of Zn with up to 3%Nd post extrusion.

Table 3. The mechanical properties as obtained from stress–strain curves of the tested alloys.

Tested Alloy	Y.P. [MPa]	UTS [MPa]	Elongation [%]
Zn-1%Nd	90 ± 0.1	135.9 ± 1.1	34.9 ± 1.5
Zn-2%Nd	91.5 ± 0.5	140.0 ± 0.4	36.7 ± 6.0
Zn-3%Nd	98.5 ± 1.5	148.9 ± 0.5	37.2 ± 1.4

The corrosion performance of the tested alloys, examined using an immersion test in a simulated physiological environment (PBS solution at 37 degrees) after 14 days, is shown in Figure 5. This reveals that the addition of up to 3%Nd has an insignificant effect on the corrosion rate of the alloys, which varied between 0.2 and 0.25 mm/year. A close-up view of the external surface of the tested alloys after immersion tests shows clear signs of micro-galvanic corrosion, as displayed within the circles in Figure 6. This was probably due to the inherent differences between the corrosion potential of the Zn-base matrix and the secondary phase $NdZn_5$, which were −1 and −1.5 V_{SCE}, respectively [44,58]. Accordingly, the Zn-matrix is more cathodic than the secondary phase, which is consequently preferably attacked by the corrosive solution. The corrosion products shown in Figure 6 were examined by EDS and XRD analysis, as shown in Table 4 and Figure 7, respectively. This mainly revealed the presence of P and Cl generated from the PBS solution and oxygen as the main ingredient of Zn-base oxide along with a minor amount of Zn-base chloride.

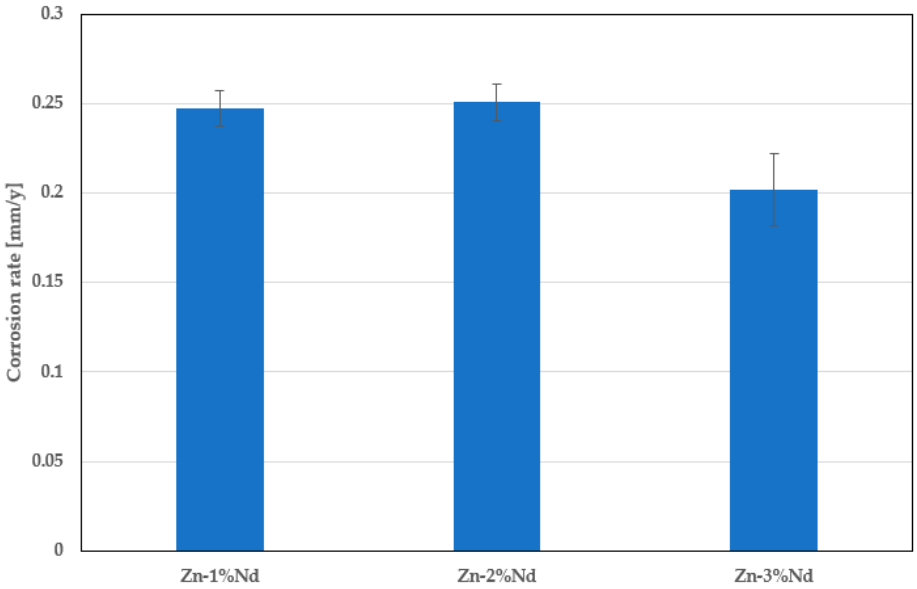


Figure 5. Corrosion rate of Zn with up to 3%Nd as obtained by immersion test in PBS solution for 14 days.

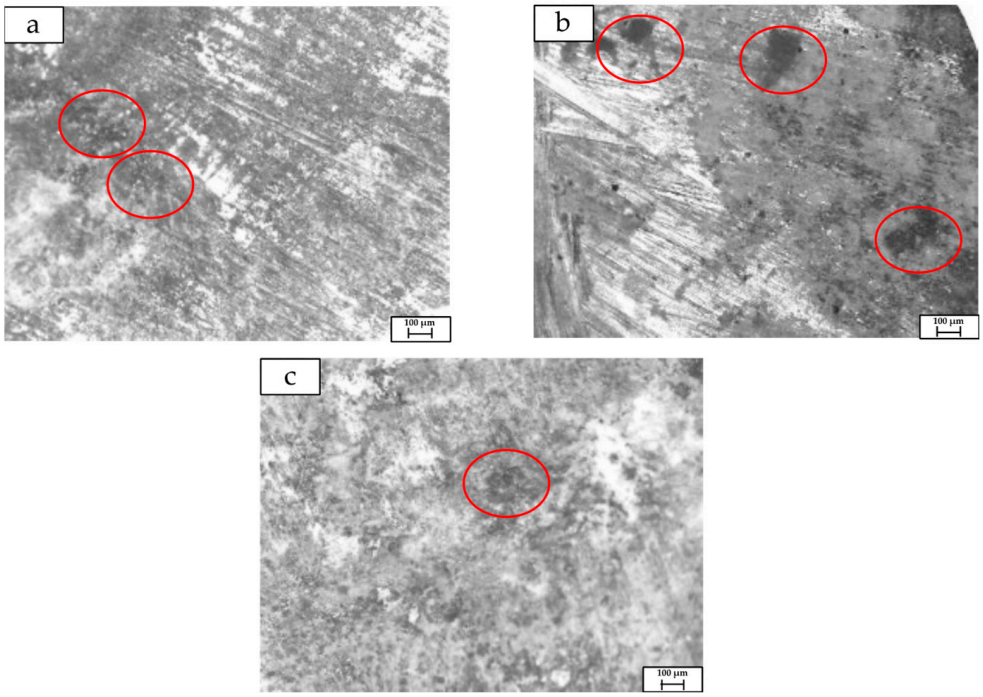


Figure 6. Typical corrosion products on the external surface of Zn with up to 3%Nd after immersion test in PBS solution for 14 days: (**a**) Zn-1%Nd; (**b**) Zn-2%Nd; (**c**) Zn-3%Nd. Corrosion product highlight by red circles.

Table 4. EDS analysis of the corrosion products (wt.%) related to Zn-3%Nd alloy.

Tested Alloy	O	P	Cl	Nd	Zn
Zn-3%Nd	18.49	9.37	0.8	3.04	Bal.

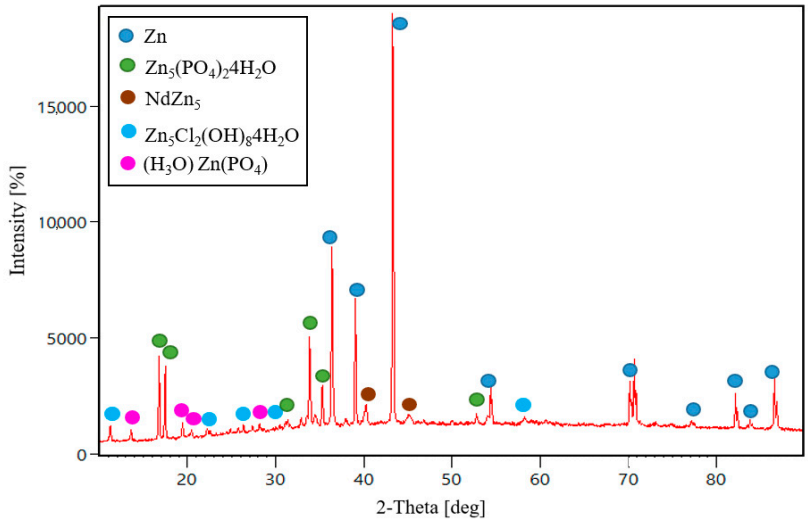


Figure 7. XRD analysis of the corrosion products related to Zn-3%Nd alloy (diffraction files: Nd 00-004-0831, $Zn_5(PO_4)_24H_2O$ 00-037-0465, $NdZn_5$ 00-027-0325, $Zn_5Cl_2(OH)_84H_2O$ 04-012-7376, (H_3O) $Zn(PO_4)$ 04-011-2320).

The electrochemical behavior of the tested alloys, examined with potentiodynamic polarization and impedance spectroscopy analysis, is shown in Figures 8 and 9, respectively, along with the derived parameters shown in Table 5. In general, the shape of the polarization curves of the tested alloys was quite similar and in accordance with the basic shape obtained by pure Zn [59]. The corrosion rates of the alloys with up to 3%Nd (0.19–0.34 mmpy) were also quite close and practically align with alloys that have fair corrosion resistance (0.1–0.5 mmpy). In terms of the corrosion potential of Zn-Nd-based alloys, similar results were obtained by Veys-Renaux et al. [60]. They also indicated that the parallel use of Ce and La reduces the Ecorr to 1.02 V. The insignificant variation between the corrosion rate of the tested alloys measured by the potentiodynamic polarization analysis and immersion tests was practically within the statistical deviation obtained by the two methods.

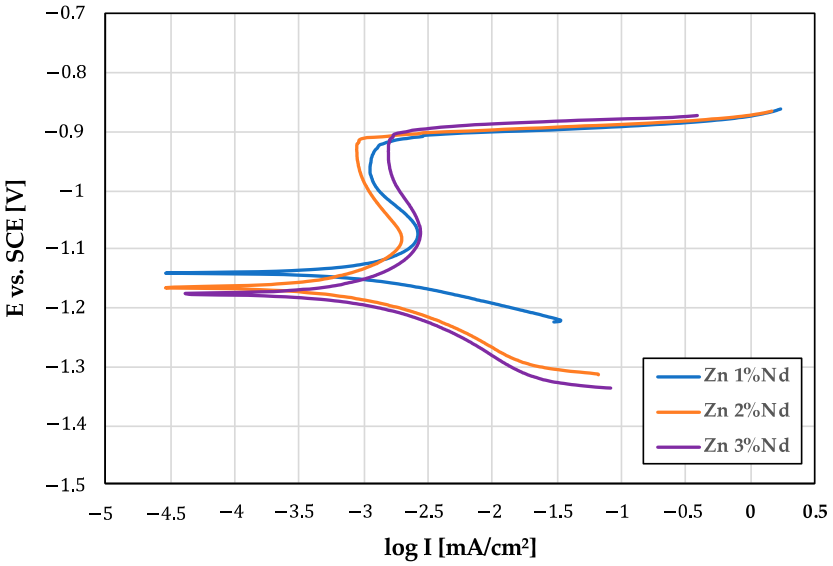


Figure 8. Potentiodynamic polarization analysis of Zn with up to 3%Nd in PBS solution.

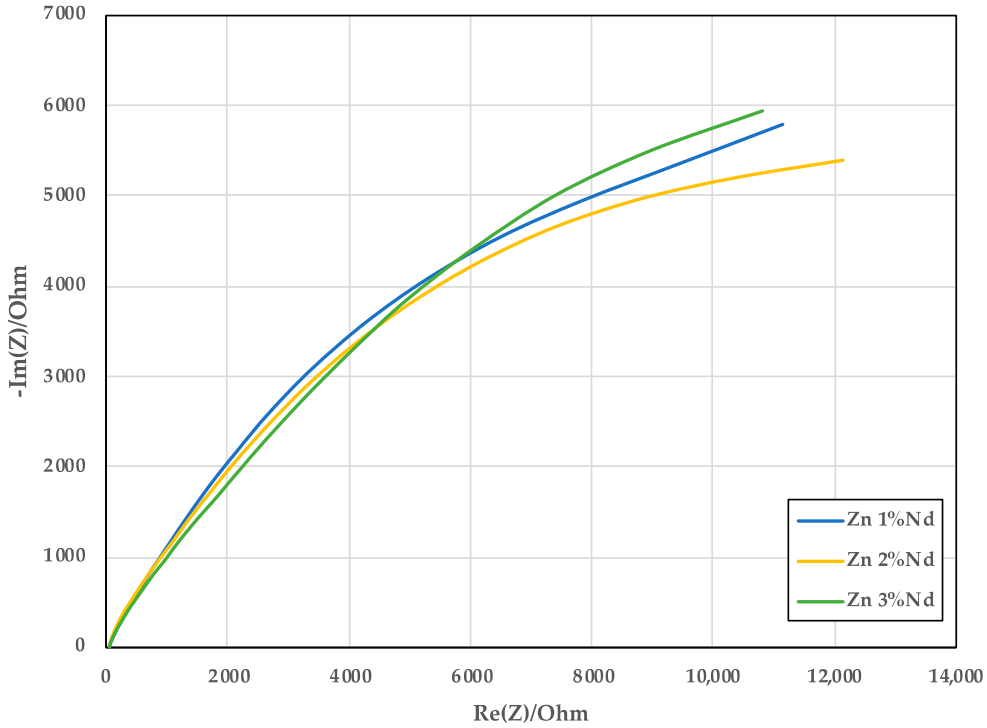


Figure 9. EIS displayed in Nyquist diagram of Zn with up to 3%Nd in PBS solution.

Table 5. Electrochemical parameters derived from Figure 8 along with corrosion rate measurements obtained by Tafel extrapolation.

Tested Alloy	Ecorr vs. SCE [V]	Icorr [μA/cm^2]	Corrosion Rate [mmpy]
Zn 1%Nd	−1.16	1.62	0.23
Zn 2%Nd	−1.2	1.34	0.19
Zn 3%Nd	−1.19	2.41	0.34

The EIS analysis, displayed in a Nyquist diagram, showed that the magnitudes of the radii of curvature of the alloys with up to 3%Nd were quite similar. Hence, as the radii of curvature represent the corrosion resistance, it can be assumed that the addition of up to 3%Nd to pure Zn has an insignificant effect on corrosion resistance. Overall, the outcome of the electrochemical assessment corresponds to the results obtained by the immersion test.

The cytotoxicity evaluation of pure Zn with up to 3%Nd, in terms of indirect cell viability analysis 24 and 48 h post incubation is shown in Figure 10. Ti-6%Al-4%V was used as a reference alloy due to its excellent biocompatibility [28]. The cytotoxicity outcome showed that the cell viability related to all the tested alloys was higher than 140% and 160% 24 and 48 h post incubation, respectively. This result was even better than the basic requirement, which claims that the cell viability should be higher than 70% (according to ISO 1099305) [56] to avoid negative cytotoxic effects relating to 4T1 cells. The cell viability of the tested alloys was also higher than the biocompatible reference alloy Ti6Al4V. In addition, the cell viability increased as the content of Nd was raised from 1 to 3%, especially after a long incubation time of 48 h. The above cell viability measurements were also in accordance with the visual healthy appearance of 4T1 cells shown in Figures 11 and 12 24 and 48 h post incubation, respectively.

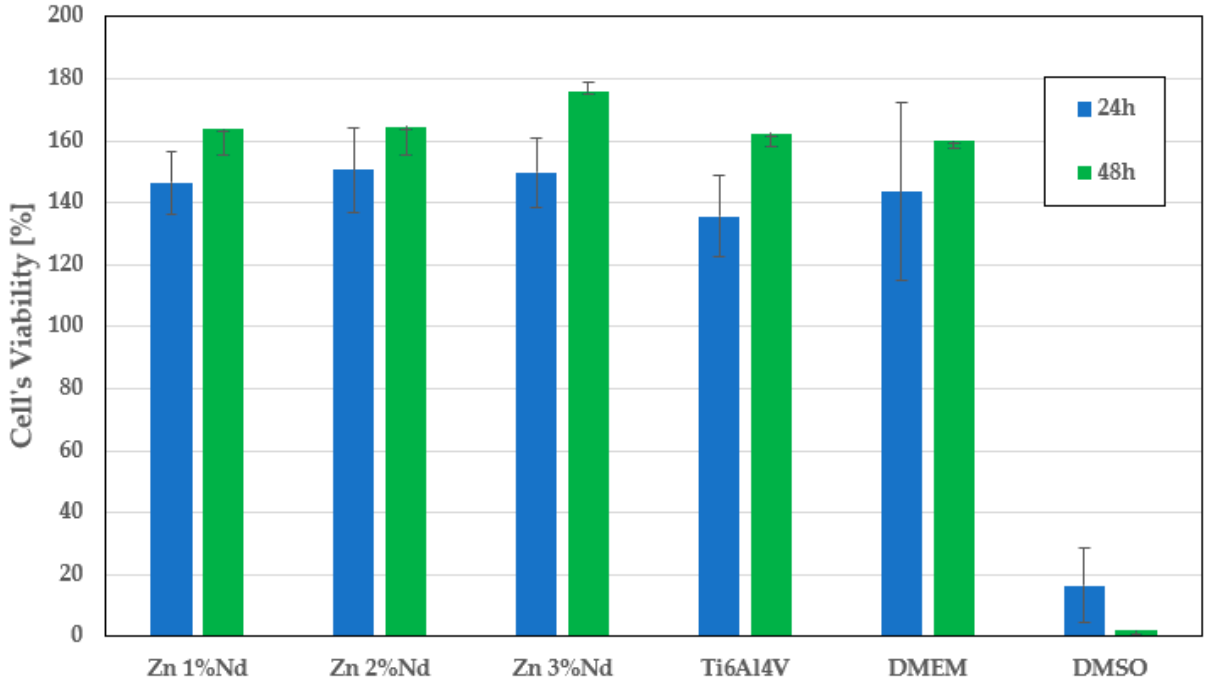


Figure 10. Indirect cell viability examination of Zn with up to 3%Nd 24 and 48 h post incubation.

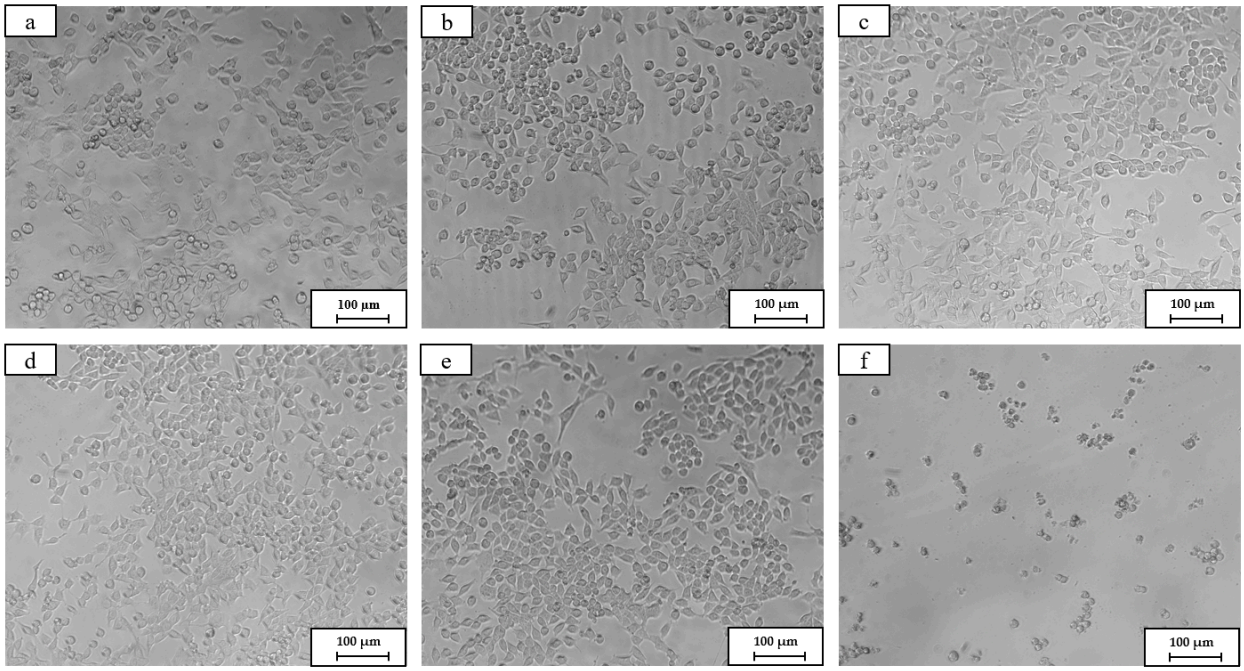


Figure 11. Typical view of 4T1 cells 24 h post incubation: (**a**) Zn-1%Nd; (**b**) Zn-2%Nd; (**c**) Zn-3%Nd; (**d**) Ti-6Al-4V; (**e**) DMEM only; (**f**) DMEM + 10% DMSO.

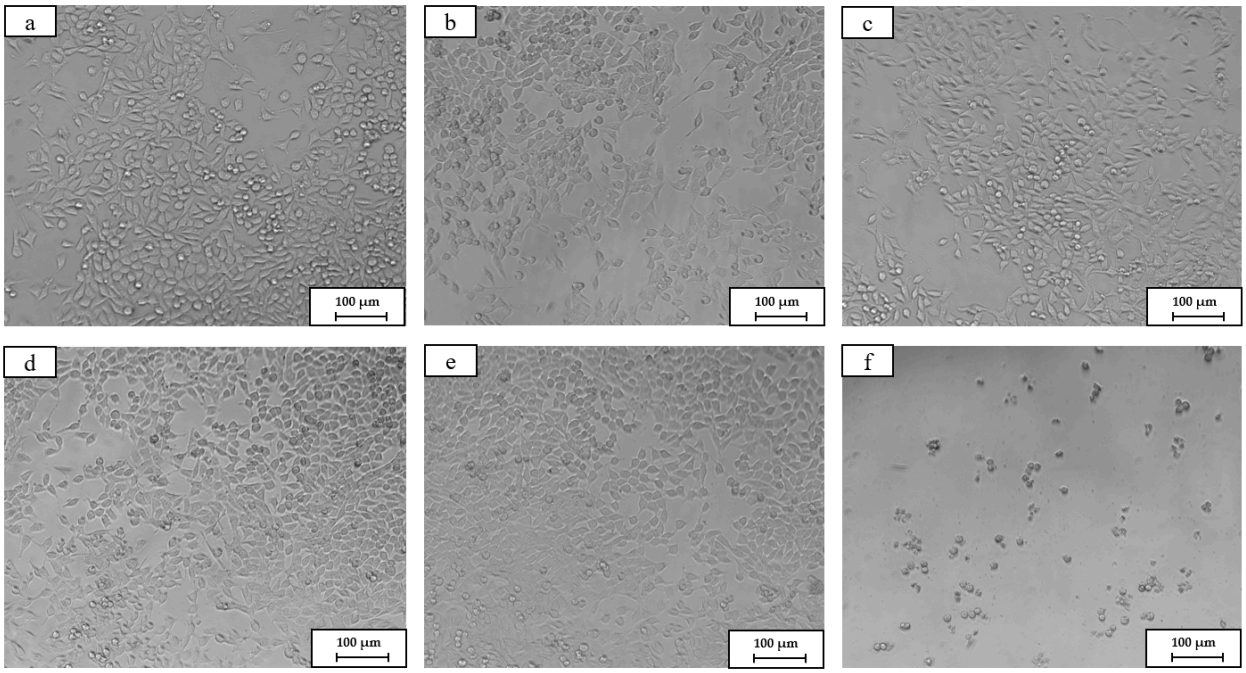


Figure 12. Overall view of 4T1 cells 48 h post incubation: (**a**) Zn-1%Nd; (**b**) Zn-2%Nd; (**c**) Zn-3%Nd; (**d**) Ti-6Al-4V; (**e**) DMEM only; (**f**) DMEM + 10% DMSO.

4. Discussion

The addition of up to 3%Nd to pure Zn has a significant reinforcing effect in terms of tension strength and hardness, with a minor effect on ductility. This was clearly demonstrated by increasing the Y.P and UTS of pure zinc (45 MPa and 50 MPa, respectively) [36], to about 90 and 135 MPa in Zn-1%Nd, 91 and 140 MPa in Zn-2%Nd, and 98 and 148 MPa in Zn-3%Nd. In terms of hardness, the hardness of pure zinc (about 40 HV) [36] was increased to about 65 HV in Zn with up to 3%Nd. Relating to ductility, the elongation of pure Zn (38%) [36] was basically maintained with only a slight reduction to 35–37% by the addition of up to 3%Nd. The strengthening effect of Nd can mainly be attributed to the formation of the secondary phase $NdZn_5$, and to the solution hardening generated by the partial dissolution of Nd in the Zn-base matrix. The fact that the ductility of the tested alloys was slightly improved (from about 35% to 37% elongation) as the Nd content was increased from 1 to 3% can be related to the effect of Nd on microstructural defects, especially in the form of porosity. This can be explained in terms of the castability capabilities of the tested alloys, as controlled by the presence of Nd. According to Shuai et al. [55], the addition of Nd to pure Zn can significantly improve the melt fluidity which consequently reduces the formation of porosity and results in an increased densification rate.

Regarding the corrosion performance of pure Zn with up to 3%Nd, examined in a simulated physiological environment (PBS solution at 37 °C), it was quite clear that Nd did not have any significant effect on the corrosion resistance. This was demonstrated in the equilibrium state conditions (immersion test), as well as in non-equilibrium conditions in terms of potentiodynamic polarization and EIS. For example, according to Kafri et al. [36], the corrosion rate of pure Zn examined by the immersion test in the same environmental conditions (PBS solution at 37 °C) was 0.21 and 0.28 mm/y after 10 and 20 days of exposure, respectively. This outcome is similar to the obtained results (corrosion rate of about 0.21–0.25 mm/y) for zinc with up to 3%Nd after 14 days of exposure to the immersion test. In terms of corrosion potential, the intrinsic variations between the Zn-base matrix and the secondary phase $NdZn_5$ are -1 V_{SCE} [44] and -1.5 V_{SCE}, [58], respectively. Accordingly, the Zn matrix is more cathodic than the secondary phase and will consequently be preferably attacked by the corrosive solution. Nevertheless, it is believed that the dynamic corrosion mechanism of zinc with up to 3%Nd is not significantly affected by the differences in the

corrosion potential between the Zn matrix and the secondary phase. This assumption is again supported by the minor differences between the corrosion rate of pure Zn and zinc with up to 3%Nd.

In terms of cytotoxicity examination, the addition of Nd has a strong favorable effect on cell viability, particularly within a prolonged incubation period (after 48 h). In general, according to Ron et al. [61], this can be mainly attributed to the inherent anti-inflammatory capabilities of Zn-base alloys. This explanation is also supported by numerous studies that highlight the anti-inflammatory characteristics of Zn [37,40,62,63]. Furthermore, the beneficial cell viability tendency related to the tested alloys was enlarged as the Nd content was increased from 1 to 3%. A convincing explanation for this phenomenon claims that Nd ions that are released throughout the degradation process have a strong affinity with the cell membrane, which subsequently inhibits the release of inflammatory cytokines.

Altogether, this in vitro study showcases the potential capability of Zn-base alloys with up to 3%Nd to act as a proper structural material for biodegradable implants. However, to accomplish this, additional in vivo assessment is essential.

5. Conclusions

1. The addition of up to 3%Nd to pure Zn has a significant strengthening effect in terms of mechanical properties and a minor favorable effect on ductility. The reinforcing effect was mainly attributed to the generation of a secondary phase $NdZn_5$.
2. In vitro corrosion assessment in simulated environmental conditions (PBS solution at 37 °C) showed that the addition of Nd did not have any deteriorating effect on the corrosion resistance.
3. Cytotoxicity assessment, in terms of indirect cell viability analysis, indicated that the tested alloys have a strong favorable effect on cell viability, particularly within prolonged incubation periods (after 48 h). This was probably mainly due to the inherent anti-inflammatory characteristics of Zn. Furthermore, the cell viability tendency was widened as the Nd content was increased from 1 to 3%.

Author Contributions: Investigation, E.H.-P., L.B.T.-M., M.B. and T.R.; formal analysis, E.H.-P.; writing—original draft preparation, E.H.-P. and E.A.; supervision, E.A.; conceptualization, E.A.; methodology, E.A. All authors have read and agreed to the published version of the manuscript.

Funding: This research received no external funding.

Institutional Review Board Statement: Not applicable.

Informed Consent Statement: Not applicable.

Data Availability Statement: The raw data supporting the conclusions of this article will be made available by the authors on request.

Conflicts of Interest: The authors declare no conflicts of interest.

References

1. Zheng, Y.F.; Gu, X.N.; Witte, F.J.M.S. Biodegradable Metals. *Mater. Sci. Eng. R Rep.* **2014**, *77*, 1–34. [CrossRef]
2. Su, Y.; Yang, H.; Gao, J.; Qin, Y.X.; Zheng, Y.; Zhu, D. Interfacial Zinc Phosphate is the Key to Controlling Biocompatibility of Metallic Zinc Implants. *Adv. Sci.* **2019**, *6*, 1900112. [CrossRef]
3. Sheikh, Z.; Najeeb, S.; Khurshid, Z.; Verma, V.; Rashid, H.; Glogauer, M. Biodegradable materials for bone repair and tissue engineering applications. *Materials* **2015**, *8*, 5744–5794. [CrossRef] [PubMed]
4. Bowen, P.K.; Shearier, E.R.; Zhao, S.; Guillory, R.J.; Zhao, F.; Goldman, J.; Drelich, J.W. Biodegradable Metals for Cardiovascular Stents: From Clinical Concerns to Recent Zn-Alloys. In *Advanced Healthcare Materials*; Wiley-VCH Verlag GmbH & Co. KGaA: Weinheim, Germany, 2016; Volume 5, pp. 1121–1140. [CrossRef]
5. Li, H.; Zheng, Y.; Qin, L. Progress of biodegradable metals. In *Progress in Natural Science: Materials International*; Elsevier: Amsterdam, The Netherlands, 2014; Volume 24, pp. 414–422. [CrossRef]
6. Liu, X.; Sun, J.; Yang, Y.; Zhou, F.; Pu, Z.; Li, L.; Zheng, Y. Microstructure, mechanical properties, in vitro degradation behavior and hemocompatibility of novel Zn-Mg-Sr alloys as biodegradable metals. *Mater. Lett.* **2016**, *162*, 242–245. [CrossRef]

7. Liu, Q.; Li, A.; Liu, S.; Fu, Q.; Xu, Y.; Dai, J.; Li, P.; Xu, S. Cytotoxicity of Biodegradable Zinc and Its Alloys: A Systematic Review. *J. Funct. Biomater.* **2023**, *14*, 206. [CrossRef]
8. Johnson, L.L.; Vandyk, G.E. Metal and Biodegradable Interference Screws: Comparison of Failure Strength. *Arthrosc. J. Arthrosc. Relat. Surg.* **1996**, *12*, 452–456. [CrossRef]
9. Levy, G.K.; Goldman, J.; Aghion, E. The Prospects of Zinc as a Structural Material for Biodegradable Implants—A Review Paper. *Metals* **2017**, *7*, 402. [CrossRef]
10. Zander, D.; Zumdick, N.A. Influence of Ca and Zn on the microstructure and corrosion of biodegradable Mg-Ca-Zn alloys. *Corros. Sci.* **2015**, *93*, 222–233. [CrossRef]
11. Králová, Z.O.; Gorejová, R.; Oriňaková, R.; Petráková, M.; Oriňak, A.; Kupková, M.; Hrubovčáková, M.; Sopčák, T.; Baláž, M.; Maskaľová, I.; et al. Biodegradable zinc-iron alloys: Complex study of corrosion behavior, mechanical properties and hemocompatibility. *Prog. Nat. Sci. Mater. Int.* **2021**, *31*, 279–287. [CrossRef]
12. Chen, H.; Zhang, E.; Yang, K. Microstructure, corrosion properties and bio-compatibility of calcium zinc phosphate coating on pure iron for biomedical application. *Mater. Sci. Eng. C* **2014**, *34*, 201–206. [CrossRef]
13. Gao, C.; Li, S.; Liu, L.; Bin, S.; Yang, Y.; Peng, S.; Shuai, C. Dual alloying improves the corrosion resistance of biodegradable Mg alloys prepared by selective laser melting. *J. Magnes. Alloys* **2021**, *9*, 305–316. [CrossRef]
14. Schinhammer, M.; Gerber, I.; Hänzi, A.C.; Uggowitzer, P.J. On the Cytocompatibility of Biodegradable Fe-Based Alloys. *Mater Sci. Eng. C Mater Biol. Appl.* **2013**, *33*, 782–789. [CrossRef]
15. Schinhammer, M.; Hänzi, A.C.; Löffler, J.F.; Uggowitzer, P.J. Design strategy for biodegradable Fe-based alloys for medical applications. *Acta Biomater.* **2010**, *6*, 1705–1713. [CrossRef]
16. Montani, M.; Demir, A.G.; Mostaed, E.; Vedani, M.; Previtali, B. Processability of pure Zn and pure Fe by SLM for biodegradable metallic implant manufacturing. *Rapid Prototyp. J.* **2017**, *23*, 514–523. [CrossRef]
17. Liu, B.; Zheng, Y.F. Effects of Alloying Elements (Mn, Co, Al, W, Sn, B, C and S) on Biodegradability and in Vitro Biocompatibility of Pure Iron. *Acta Biomater.* **2011**, *7*, 1407–1420. [CrossRef] [PubMed]
18. Kafri, A.; Ovadia, S.; Yosafovich-Doitch, G.; Aghion, E. The Effects of 4%Fe on the Performance of Pure Zinc as Biodegradable Implant Material. *Ann. Biomed. Eng.* **2019**, *47*, 1400–1408. [CrossRef] [PubMed]
19. Rivkin, B.; Akbar, F.; Otto, M.; Beyer, L.; Paul, B.; Kosiba, K.; Gustmann, T.; Hufenbach, J.; Medina-Sánchez, M. Remotely Controlled Electrochemical Degradation of Metallic Implants. *Small* **2024**. *Online Version of Record*. [CrossRef] [PubMed]
20. Lee, H.H.; Hiam, D. Corrosion Resistance of Galvannealed Steel. *Corrosion* **1989**, *45*, 852–856. [CrossRef]
21. Esmaily, M.; Svensson, J.; Fajardo, S.; Birbilis, N.; Frankel, G.; Virtanen, S.; Arrabal, R.; Thomas, S.; Johansson, L.-G. Fundamentals and Advances in Magnesium Alloy Corrosion. *Prog. Mater. Sci.* **2017**, *89*, 2169. [CrossRef]
22. Gu, X.N.; Zheng, Y.F. A review on magnesium alloys as biodegradable materials. *Front. Mater. Sci. China* **2010**, *4*, 111–115. [CrossRef]
23. Li, H.F.; Shi, Z.Z.; Wang, L.N. Opportunities and challenges of biodegradable Zn-based alloys. *J. Mater. Sci. Technol.* **2020**, *46*, 136–138. [CrossRef]
24. Staiger, M.; Pietak, A.; Huadmai, J.; Biomaterials, G.D. Magnesium and Its Alloys as Orthopedic Biomaterials: A Review. *Biomaterials* **2006**, *27*, 1728–1734–1734. [CrossRef] [PubMed]
25. Kafri, A.; Ovadia, S.; Yosafovich-Doitch, G.; Aghion, E. In Vivo Performances of Pure Zn and Zn–Fe Alloy as Biodegradable Implants. *J. Mater. Sci. Mater. Med.* **2018**, *29*, 94. [CrossRef] [PubMed]
26. Frank, W. The History of Biodegradable Magnesium Implants: A Review. *Acta Biomater.* **2010**, *6*, 1680–1692.
27. Aghion, E.; Gueta, Y.; Moscovitch, N.; Bronfin, B. Effect of Yttrium Additions on the Properties of Grain-Refined Mg-3%Nd Alloy. *J. Mater. Sci.* **2008**, *43*, 4870–4875. [CrossRef]
28. Avior, O.; Ghedalia-Peled, N.b.; Ron, T.; Metals, R.V. The Effect of ca on in Vitro Behavior of Biodegradable Zn-Fe Alloy in Simulated Physiological Environments. *Metals* **2020**, *10*, 1624. [CrossRef]
29. Jia, B.; Yang, H.; Han, Y.; Zhang, Z.; Qu, X.; Zhuang, Y.; Wu, Q.; Zheng, Y.; Dai, K. In vitro and in vivo studies of Zn-Mn biodegradable metals designed for orthopedic applications. *Acta Biomater.* **2020**, *108*, 358–372. [CrossRef] [PubMed]
30. Tong, X.; Zhang, D.; Zhang, X.; Su, Y.; Shi, Z.; Wang, K.; Lin, J.; Li, Y.; Lin, J.; Wen, C. Microstructure, mechanical properties, biocompatibility, and in vitro corrosion and degradation behavior of a new Zn–5Ge alloy for biodegradable implant materials. *Acta Biomater.* **2018**, *82*, 197–204. [CrossRef] [PubMed]
31. Sikora-Jasinska, M.; Mostaed, E.; Mostaed, A.; Beanland, R.; Mantovani, D.; Vedani, M. Fabrication, mechanical properties and in vitro degradation behavior of newly developed Zn[sbnd]Ag alloys for degradable implant applications. *Mater. Sci. Eng. C* **2017**, *77*, 1170–1181. [CrossRef]
32. Tang, Z.; Niu, J.; Huang, H.; Zhang, H.; Pei, J.; Ou, J.; Yuan, G. Potential biodegradable Zn-Cu binary alloys developed for cardiovascular implant applications. *J. Mech. Behav. Biomed. Mater.* **2017**, *72*, 182–191. [CrossRef]
33. Sun, S.; Ren, Y.; Wang, L.; Yang, B.; Li, H.; Qin, G. Abnormal effect of Mn addition on the mechanical properties of as-extruded Zn alloys. *Mater. Sci. Eng. A* **2017**, *701*, 129–133. [CrossRef]
34. Kubásek, J.; Vojtěch, D.; Jablonská, E.; Pospíšilová, I.; Lipov, J.; Ruml, T. Structure, mechanical characteristics and in vitro degradation, cytotoxicity, genotoxicity and mutagenicity of novel biodegradable Zn-Mg alloys. *Mater. Sci. Eng. C* **2016**, *58*, 24–35. [CrossRef]

35. Zou, Y.; Chen, X.; Chen, B. Effects of Ca concentration on degradation behavior of Zn-x Ca alloys in Hank's solution. *Mater. Lett.* **2018**, *218*, 193–196. [CrossRef]
36. Kafri, A.; Ovadia, S.; Goldman, J.; Drelich, J.; Aghion, E. The suitability of Zn-1.3%Fe alloy as a biodegradable implant material. *Metals* **2018**, *8*, 153. [CrossRef]
37. Berg, J.M.; Shi, Y. The Galvanization of Biology: A Growing Appreciation for the Roles of Zinc. *Science* **1996**, *271*, 1081–1085. [CrossRef] [PubMed]
38. Mostaed, E.; Sikora-Jasinska, M.; Mostaed, A.; Loffredo, S.; Demir, A.G.; Previtali, B.; Mantovani, D.; Beanland, R.; Vedani, M. Novel Zn-based alloys for biodegradable stent applications: Design, development and in vitro degradation. *J. Mech. Behav. Biomed. Mater.* **2016**, *60*, 581–602. [CrossRef]
39. Zhu, D.; Cockerill, I.; Su, Y.; Zhang, Z.; Fu, J.; Lee, K.W.; Ma, J.; Okpokwasili, C.; Tang, L.; Zheng, Y.; et al. Mechanical strength, biodegradation, and in vitro and in vivo biocompatibility of Zn biomaterials. *ACS Appl. Mater. Interfaces* **2019**, *11*, 6809–6819. [CrossRef]
40. Wei, Z.; Burwinkel, M.; Palissa, C.; Ephraim, E.; Schmidt, M.F. Antiviral activity of zinc salts against transmissible gastroenteritis virus in vitro. *Veter-Microbiol.* **2012**, *160*, 468–472. [CrossRef]
41. Gabay, N.; Ron, T.; Vago, R.; Shirizly, A.; Materials, E.A. Evaluating the Prospects of Ti-Base Lattice Infiltrated with Biodegradable Zn-2% Fe Alloy as a Structural Material for Osseointegrated Implants—In Vitro Study. *Materials* **2021**, *14*, 4682. [CrossRef]
42. Wang, X.M.; Lu, G.J.; Cui, L.Y.; Liu, C.B.; Kannan, M.B.; Zhang, F.; Li, S.Q.; Zou, Y.H.; Zeng, R.C. In vitro degradation and biocompatibility of vitamin C loaded Ca-P coating on a magnesium alloy for bioimplant applications. *Corros. Commun.* **2022**, *6*, 16–28. [CrossRef]
43. Cai, L.; Guo, H.-R.; Zhu, Y.-Q.; Du, F.-S.; Qi, J.-T.; Cui, L.-Y.; Liu, C.-B.; Zeng, R.-C. Biodegradation mechanisms of pure Mg in presence of glucose, vitamin C, and citric acid. *Smart Mater. Manuf.* **2023**, *1*, 100014. [CrossRef]
44. Ben Tzion-Mottye, L.; Ron, T.; Eliezer, D.; Aghion, E. The Effect of Mn on the Mechanical Properties and In Vitro Behavior of Biodegradable Zn-2%Fe Alloy. *Metals* **2022**, *12*, 1291. [CrossRef]
45. Stroganov, G.B.; Savitski, E.M.; Tikhov, N.M.; Terekhova, V.F.; Volkov, M.V.; Sivash, K.M.; Borodkin, V.S. U.S. Patent 3687135, 29 August 1972.
46. Quach, N.C.; Uggowitzer, P.J.; Schmutz, P. Corrosion behaviour of an Mg–Y–RE alloy used in biomedical applications studied by electrochemical techniques. *Comptes Rendus. Chim.* **2008**, *11*, 1043–1054. [CrossRef]
47. Du, S.; Shen, Y.; Zheng, Y.; Cheng, Y.; Xu, X.; Chen, D.; Xia, D. Systematic in vitro and in vivo study on biodegradable binary Zn-0.2 at% Rare Earth alloys (Zn-RE: Sc, Y, La-Nd, Sm-Lu). *Bioact. Mater.* **2023**, *24*, 507–523. [CrossRef] [PubMed]
48. Kim, Y.-S.; Lim, C.-H.; Shin, S.-H.; Kim, J.-C. Twenty-Eight-Day Repeated Inhalation Toxicity Study of Nano-Sized Neodymium Oxide in Male Sprague-Dawley Rats. *Toxicol. Res.* **2017**, *33*, 239–253. [CrossRef] [PubMed]
49. Cheng, J.; Cheng, Z.; Hu, R.; Cui, Y.; Cai, J.; Li, N.; Gui, S.; Sang, X.; Sun, Q.; Wang, L.; et al. Immune dys-function and liver damage of mice following exposure to lanthanoids. *Environ. Toxicol.* **2014**, *29*, 64–73. [CrossRef] [PubMed]
50. Shi, Z.; Yu, J.; Liu, X.F. Microalloyed Zn-Mn Alloys: From Extremely Brittle to Extraordinarily Ductile at Room Temperature. *Mater. Des.* **2018**, *144*, 343–352. [CrossRef]
51. Wang, J.; Witte, F.; Xi, T.; Zheng, Y.; Yang, K.; Yang, Y.; Zhao, D.; Meng, J.; Li, Y.; Li, W.; et al. Recommendation for Modifying Current Cytotoxicity Testing Standards for Biodegradable Magnesium-Based Materials. *Acta Biomater.* **2015**, *21*, 237–249. [CrossRef] [PubMed]
52. Kaya, A.A.; Uzan, P.; Eliezer, D.; Aghion, E. Electron microscopical investigation of as cast AZ91D alloy. *Mater. Sci. Technol.* **2000**, *16*, 1001–1006. [CrossRef]
53. Vander Voort, G.F. *Metallography, Principles and Practice*; ASM International: Almere, The Netherlands, 1999.
54. Leon, A.; Shirizly, A.; Aghion, E. Corrosion behavior of AlSi10Mg alloy produced by additive manufacturing (AM) vs. Its counterpart gravity cast alloy. *Metals* **2016**, *6*, 148. [CrossRef]
55. Proksch, E. pH in nature, humans and skin. *J. Dermatol.* **2018**, *45*, 1044–1052. [CrossRef] [PubMed]
56. *ISO 10993-12*; Biological Evaluation of Medical Devices—Part 12: Sample Preparation and Reference Materials. International Organization for Standardization (ISO): Geneva, Switzerland, 2012.
57. Shuai, C.J.; Yang, M.l.; Deng, F.; Yang, Y.W.; Peng, S.P.; Qi, F.W.; He, C.X.; Shen, L.D.; Liang, H.x. Forming quality, mechanical properties, and anti-inflammatory activity of additive manufactured Zn-Nd alloy. *J. Zhejiang Univ. Sci. A* **2020**, *21*, 876–891. [CrossRef]
58. Cabibbo, M.; Paoletti, C.; Minárik, P.; Král, R.; Zemková, M. Secondary phase precipitation and thermally stable microstructure refinement induced by ECAP on Mg-Y-Nd (WN43) alloy. *Mater. Lett.* **2019**, *237*, 5–8. [CrossRef]
59. Dutra, C.A.M.; Codaro, E.N.; Nakazato, R.Z. Electrochemical behavior and corrosion study of electrodeposits of Zn and Zn-Fe-Co on steel. *Mater. Sci. Appl.* **2012**, *3*, 348–354.
60. Veys-Renaux, D.; Guessoum, K.; Rocca, E.; David, N.; Belhamel, K. New zinc-rare earth alloys: Influence of intermetallic compounds on the corrosion resistance. *Corros. Sci.* **2013**, *77*, 342–349. [CrossRef]
61. Ron, T.; Leon, A.; Kafri, A.; Ashraf, A.; Na, J.; Babu, A.; Banerjee, R.; Brookbank, H.; Muddaluri, S.; Little, K.; et al. Nerve regeneration with a scaffold incorporating an absorbable Zinc-2% Iron alloy filament to improve axonal guidance. *Pharmaceutics* **2023**, *15*, 2595. [CrossRef]

62. Peng, F.; Xie, J.; Liu, H.; Zheng, Y.; Qian, X.; Zhou, R.; Zhong, H.; Zhang, Y.; Li, M. Shifting focus from bacteria to host neutrophil extracellular traps of biodegradable pure Zn to combat implant centered infection. *Bioact. Mater.* **2023**, *21*, 436–449. [CrossRef]
63. Thian, E.S.; Konishi, T.; Kawanobe, Y.; Lim, P.N.; Choong, C.; Ho, B.; Aizawa, M. Zinc-substituted hydroxyapatite: A biomaterial with enhanced bioactivity and antibacterial properties. *J. Mater. Sci. Mater. Med.* **2013**, *24*, 437–445. [CrossRef]

Disclaimer/Publisher's Note: The statements, opinions and data contained in all publications are solely those of the individual author(s) and contributor(s) and not of MDPI and/or the editor(s). MDPI and/or the editor(s) disclaim responsibility for any injury to people or property resulting from any ideas, methods, instructions or products referred to in the content.